Astronomy & Astrophysics manuscript no. ms_final
November 13, 2025

Letter to the Editor

Variability of optical spectral index to support a central sub-parsec binary black hole system in quasar SDSS J001224-102226.51

XueGuang Zhang

Guangxi Key Laboratory for Relativistic Astrophysics, School of Physical Science and Technology, GuangXi University, No. 100, Daxue Road, Nanning, 530004, P. R. China e-mail: xgzhang@gxu.edu.cn

November 13, 2025

ABSTRACT

In this manuscript, variations in optical spectral index α_{5100} are applied for detecting central sub-parsec binary black hole systems (sub-pc BBHs) in broad line active galactic nuclei (BLAGN), due to apparent effects of obscurations on central two BH accreting systems. For sub-pc BBHs in BLAGN, two main characteristics on α_{5100} can be expected. First, if a BLAGN harbours a central sub-pc BBH, the expected unique variability in α_{5100} should lead the BLAGN to be an outlier in the space of α_{5100} versus continuum luminosity L_{5100} determined from normal BLAGN. Second, BLAGN harbouring central sub-pc BBHs could lead to periodic variations in α_{5100}. Here, after checking the two-epoch SDSS spectra of quasar SDSS J0012-1022 reported as a candidate of sub-pc BBH by large velocity offset between narrow and broad Balmer emission lines, unique variability of α_{5100} can be explained by effects of obscurations related to an assumed central sub-pc BBH. In the near future, to detect and report periodic variations of α_{5100} for sub-pc BBHs in BLAGN should be our main objective. The results provide a new method by applications of properties of optical continuum emissions for detecting sub-pc BBHs in BLAGN.

Key words. galaxies:active - galaxies:nuclei - quasars: supermassive black holes - transient events: QPOs

1. Introduction

Sub-parsec binary black hole systems (sub-pc BBHs) in broad line active galactic nuclei (BLAGN) have been accepted as main targets for gravitational wave signals at nano-Hz frequencies (Foster & Backer 1990; Arzoumanian et al. 2015; Sesana et al. 2018; Izquierdo-Villalba et al. 2022; Reardon et al. 2023; Petrov et al. 2024; Somalwar et al. 2025; Truant et al. 2025), to provide further clues on final stages of BH merging as discussed in Begelman et al. (1980); Mayer et al. (2010); Fragione et al. (2019); Mannerkoski et al. (2022); Avara et al. (2024). Therefore, it is necessary and meaningful to detect more candidates of sub-pc BBHs.

Different methods have been proposed for detecting sub-pc BBHs in BLAGN through properties of photometric variability and spectroscopic features. Considering long-standing optical Quasi-Periodic Oscillations (QPOs) with periodicities around hundreds to thousands of days related to orbital motions of sub-pc BBHs, optical QPOs detected in photometric variability have been accepted as indicators for sub-pc BBHs, as reported in Graham et al. (2015a,b); Charisi et al. (2016); Zheng et al. (2016); Zhang (2022a,b, 2023a, 2025a,c). Meanwhile, unique properties of spectroscopic emission line features have been applied to detect sub-pc BBHs. Eracleous et al. (2012) have reported a sample of sub-pc BBH candidates through broad Hβ emission lines displaced from narrow emission lines with shifted velocities larger than 1000km/s. Boroson & Lauer (2009) have reported the sub-pc BBH candidate in SDSS J1536+0441 through unique double-peaked features in broad emission lines. Zhang (2021, 2023b, 2025b) have reported the sub-pc BBH candidates in SDSS J1547, SDSS J1257 and PG 1411+442 through different line profiles of broad Balmer emission lines.

Besides expected unique spectroscopic emission line properties, the intrinsic dependence of broad line luminosity on continuum luminosity (Greene & Ho 2005) should indicate spectroscopic continuum emissions (such as spectral index) in multi-epoch spectra could also provide efficient clues to support sub-pc BBHs in BLAGN. Therefore, to detect and report such clues is the main objective of the manuscript. Here, only the sub-pc BBHs with separation large enough are mainly considered, with little contribution of circum-binary disk (Noble et al. 2012; D'Orazio et al. 2015; Bowen et al. 2017; Noble et al. 2021; Avara et al. 2024) to the optical continuum emissions.

In this manuscript, Section 2 presents the spectroscopic results and main discussions of the BLAGN SDSS J001224-102226.51 (=SDSS J0012-1022) at redshift 0.228 reported in Eracleous et al. (2012), showing unique variability properties of optical spectral index, providing further clues to support a central sub-pc BBH. Section 3 shows necessary discussions on optical QPOs in gr-band light curves from Zwicky Transient Facility (ZTF) (Bellm et al. 2019; Masci et al. 2019) in SDSS J0012-1022. Main conclusions are given in Section 4. Throughout the manuscript, we have adopted the cosmological parameters of H_0=70 km s^{-1} Mpc^{-1}, Ω_m=0.3, and Ω_Λ=0.7.

2. Spectroscopic results for SDSS J0012-1022

Considering normal BLAGN, there is an apparent dependence of optical spectral index α_{5100} ($f_\lambda \propto \lambda^{\alpha_{5100}}$) underneath broad H$\beta$ on continuum luminosity at 5100Å L_{5100}, as shown in top panel of Fig. 1 for the selected 3274 low redshift ($z < 0.35$) SDSS quasars in Shen et al. (2011) with reliable measurements of α_{5100} (between -5 and 3) and L_{5100} (5 times larger than corresponding uncertainties), with Spearman rank correlation coefficient

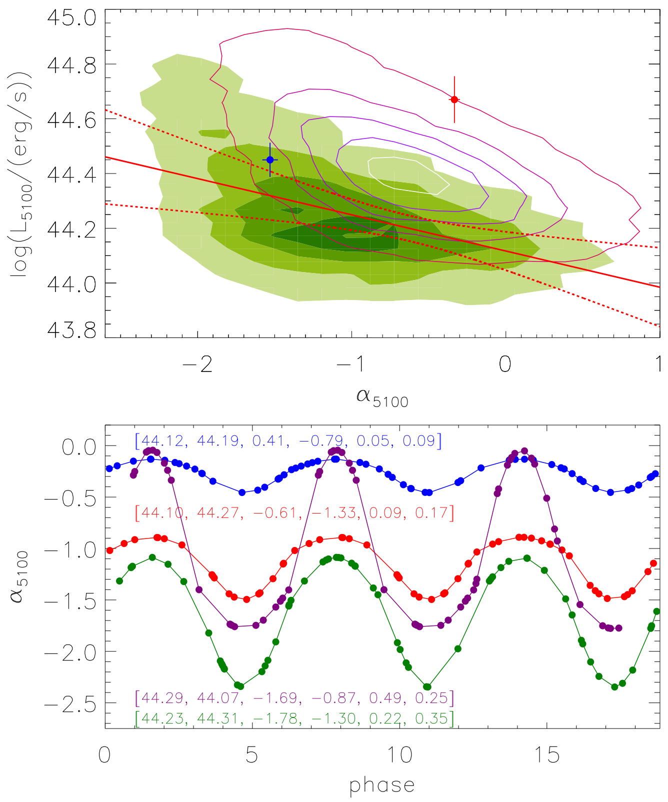

Fig. 1. Top panel shows the contour (filled by greenish colors) for the correlation between L_{5100} and α_{5100} of the selected 3274 SDSS quasars. Circles plus error bars in blue and in red show the results of SDSS J0012-1022 with MJD=52141 and 56628. Solid and dashed lines in red show the best fitting results and corresponding 5σ confidence bands. Contour with reddish levels represents the results through the 20000 artificial f_λ. The contour levels in each contour represent 0.1, 0.3, 0.5, 0.7 and 0.9 of the 2D volume contained. Bottom panel shows four examples on periodic variations in α_{5100} related to sub-pc BBHs, with corresponding model parameters listed in the same color. The six parameters in each square bracket are $\log(L_1)$, $\log(L_2)$, α_1, α_2, E_{10} and E_{20}.

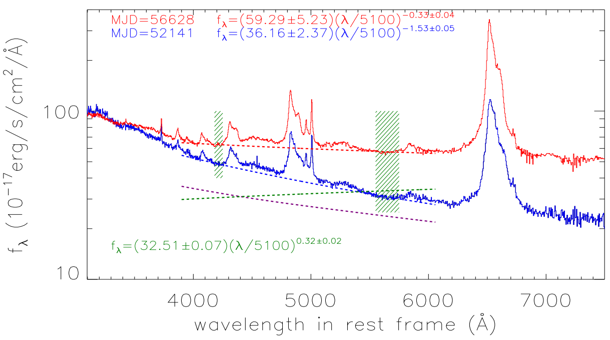

Fig. 2. SDSS spectra of SDSS J0012-1022 with MJD = 52141 (in blue) and 56628 (in red). Dashed lines in blue and in red show the power law function determined optical continuum emissions underneath broad Hβ through the two regions filled by dark green lines. Dashed purple line represents the first component related to the obscured power law component shown as dashed blue line with E(B-V)=0.1, and dashed dark green line shows the second component (formula listed in dark green characters) from the other one BH accreting system. The sum of the two components is one solution related to a sub-pc BBH to the continuum emissions in the spectrum with MJD=56628.

-0.51 ($P_{null} < 10^{-10}$). After considering uncertainties in both coordinates, through the Least Trimmed Squares regression technique (Cappellari et al. 2013), the dependence can be described as $\log \frac{L_{5100}}{\mathrm{erg/s}} = (44.117 \pm 0.005) - (0.132 \pm 0.004)\alpha_{5100}$ with RMS scatter of 0.149. The results are consistent with results in Paltani & Courvoisier (1994); Schmidt et al. (2023); Patel et al. (2025) that vast majority of BLAGN get bluer when they get brighter.

Once assumed a sub-pc BBH in a BLAGN, different obscurations on continuum emissions related to two BH accreting systems could be naturally expected, and inevitably have a strong dependence on inclination angle. If one BLAGN harbouring a sub-pc BBH should have unique variability in optical spectral index, leading the BLAGN to be an outlier in the space of α_{5100} versus L_{5100} for the normal quasars, such as the following discussed results in SDSS J0012-1022.

SDSS J0012-1022 is a quasar at redshift 0.228 in Sloan Digital Sky Survey (SDSS) (Almeida et al. 2023), with its high-quality SDSS spectra (plate-mjd-fiberid=0651-52141-0072 and 7169-56628-0344) observed at MJD=52141 and 56628 shown in Fig. 2. The power law continuum emissions $f_\lambda = A(\frac{\lambda}{5100})^{\alpha_{5100}}$ underneath broad Hβ can be determined by the continuum emissions with rest wavelength from 4180 to 4250Å and from 5550 to 5750Å through the Levenberg-Marquardt least-squares minimization technique (Markwardt 2009), leading to $A = 36.16 \pm 2.37$ $\alpha_{5100} = -1.53 \pm 0.05$ and $A = 59.29 \pm 5.23$, $\alpha_{5100} = -0.33 \pm 0.04$ for the spectrum with MJD=52141 and 56628, respectively. In top panel of Fig. 1, the determined α_{5100} and L_{5100} lead SDSS J0012-1022 with MJD=52141 (solid blue circle) to lie in the common region in the space of α_{5100} versus L_{5100} for normal quasars, however, the determined values with MJD=56628 apparently lead SDSS J0012-1022 (solid red circle) to be an outlier having opposite behaviour in the space. In other words, when SDSS J0012-1022 got brighter from MJD=52141 to 56628, there was not bluer but redder continuum emissions around 5100Å.

Based on the results in top panel of Fig. 1 for SDSS J0012-1022, obscurations on optical continuum emissions in normal BLAGN cannot be accepted. Then, we check whether an assumed sub-pc BBH can be applied.

For an assumed sub-pc BBH, observed optical continuum emissions $f(\lambda)$ (λ from 4400Å to 5600Å in rest frame) actually include two sources of $f_1(\lambda, ob)$ and $f_2(\lambda, ob)$ with different spectral indices from central two BH accreting systems,

$$f(\lambda) = f_1(\lambda, ob) + f_2(\lambda, ob) = k_1(\lambda, \phi) f_1(\lambda) + k_2(\lambda, \phi) f_2(\lambda) \quad (1)$$

, with $k_1(\lambda, \phi)$ and $k_2(\lambda, \phi)$ (ϕ as orbital phase) representing effects of obscurations on intrinsic $f_1(\lambda) \propto (\lambda/5100)^{\alpha_1}$ (continuum luminosity L_1 at 5100Å) and $f_2(\lambda) \propto (\lambda/5100)^{\alpha_2}$ (continuum luminosity L_2 at 5100Å).

Meanwhile, $k_1(\lambda, \phi)$ and $k_2(\lambda, \phi)$ can be simply determined by evolutions of color excess E(B-V) simply described by the following periodic functions

$$\begin{aligned} E_1(B-V, \phi) &= E_{10} \times |sin(\phi)| \;\; (\phi \in [\phi_1,\ \phi_2]) \\ E_1(B-V, \phi) &= 0 \;\; (\phi \in [0,\ \phi_1]\ \ or\ [\phi_2,\ 2\pi]) \\ E_2(B-V, \phi) &= E_{20} \times |sin(\phi)| \;\; (\phi \in [0,\ \phi_1]\ \ or\ [\phi_2,\ 2\pi]) \\ E_2(B-V, \phi) &= 0 \;\; (\phi \in [\phi_1,\ \phi_2]) \end{aligned} \quad . \quad (2)$$

The parameters of ϕ_1 and ϕ_2 ($0 \leq (\phi_2 - \phi_1) \leq \pi$) are applied to determine the phase information for existence of covered regions of one BH accreting system by the other system. And, the extinction curve in Fitzpatrick (1999) has been accepted. Then, assumed sub-pc BBHs, artificial $f(\lambda)$ can be created by the following steps.

First, among the 3274 SDSS quasars shown in top panel of Fig. 1, two quasars are random selected, leading to the measured values of the two quasars as the intrinsic L_1, α_1 and L_2, α_2. Second, according to the redshift of one of the two selected quasars in the first step, $f_1(\lambda)$ and $f_2(\lambda)$ can be described as

$$f_i(\lambda) = \frac{L_i}{4\pi \times 5100 \times D^2}(\frac{\lambda}{5100})^{\alpha_i} \quad (i = 1, 2) \tag{3}$$

with D as the redshift determined luminosity distance. Third, ϕ_1 and $2\pi > \phi_2 > \phi_1$ are randomly selected from 0 to π and from 0 to 2π, and E_{10} and E_{20} are randomly selected from 0 to 0.5, leading to determined $k_1(\lambda, \phi)$ and $k_2(\lambda, \phi)$. Here, the sampled range of E_{10} and E_{20} not only covers differences in spectral index of the emitting sources, but also accounts for a wide range of physical factors inherent to observing a sample of different orbiting systems. Then, the artificial $f(\lambda)$ can be obtained by equations above. Fourth, through the least-squares minimization technique, a power law function $A(\frac{\lambda}{5100})^{\alpha_A}$ applied to describe the artificial $f(\lambda)$ can lead to the determined spectral index α_A and the continuum luminosity L_A at 5100Å. Finally, repeating the steps above 20000 times, a sample of 20000 artificial $f(\lambda)$ can be created.

The dependence of L_A on α_A is also shown in top panel of Fig. 1 for the 20000 artificial $f(\lambda)$, apparently leading to the dependence of L_A on α_A moving to the upper right. Actually, we have checked effects of different values of E_{10} and E_{20} and different periodic functions applied to describe $E(B - V, \phi)$, leading to similar results, but with more or less extended areas with lower L_A. Therefore, SDSS J0012-1022 having unique variability in α_{5100} as an outlier having opposite behaviour in the space of L_{5100} versus α_{5100} can be explained by an assumed sub-pc BBH, mainly due to SDSS J0012-1022 well covered by the space of L_A versus α_A.

Before ending the section, five points should be noted. First, if the time duration 4487 days from MJD=52141 to 56628 of the two SDSS spectra of SDSS J0012-1022 is exactly an integer multiple of the orbital period of the assumed sub-pc BBH, the discussions above cannot be accepted, due to the same spatial structures for the two BH accreting systems at the two epochs. Therefore, it is necessary to check the orbital period in SDSS J0012-1022 related to an assumed sub-pc BBH. Second, through the procedure above with ϕ randomly from 0 to 6π, periodic variations of spectral index should be expected, such as the shown examples in bottom panel of Fig. 1 (the example in purple with α_{5100} varying from -1.78 to -0.04, larger than the varying range in α_{5100} in SDSS J0012-1022), indicating a new method for detecting sub-pc BBHs in BLAGN through periodic variation in spectral index. Third, for assumed sub-pc BBHs, Fig. 2 shows a solution to the continuum emissions with MJD=56628 in SDSS J0012-1022, with detailed descriptions in Appendix A. Fourth, we have assumed continuum emissions from central two BH accreting systems to be similar as those of individual normal quasars. Actually, if considering modifications related to BBHs, further evidence can be found to better support our conclusions, as detailed descriptions in Appendix B. Fifth, in order to provide further clues on importance of periodic obscurations on our conclusions, constant extinctions with $E_1(B - V, \phi) = E_2(B - V, \phi) = E_0$ have been considered in the same procedure above, as detailed descriptions in the Appendix C, to further confirm periodic obscurations related to orbital motions as key roles for unique variability properties of optical spectral index in BLAGN if harbouring sub-pc BBHs.

3. Optical QPOs in SDSS J0012-1022

The 6.3 years-long ZTF gr-band light curves are shown in left panel of Fig. 3 with $t = MJD - 58200$ from 88 to 2411. Based on applications of a base line plus a sine component

$$LC(t) = A \times \sin(\frac{2\pi \times t}{T_p} + \phi_0) + \begin{cases} B_0 & (t < 800) \\ C_0 & (t > 800) \end{cases} \tag{4}$$

through the least-squares minimization technique, the best fitting results with $\chi^2/dof \sim 5.5$ to the gr-band light curves can lead to the determined optical periodicity 827±2 days. Here, due to about 0.2-0.25 magnitudes darker in the LC with $t < 800$ than in the LC with $t > 800$, two different base lines B_0 and C_0 are applied for the LC with $t < 800$ and with $t > 800$.

Meanwhile, the commonly accepted Lomb-Scargle (LS) periodogram (Zechmeister & Kurster 2009; VanderPlas 2018) has been applied to the ZTF gr-band light curves of SDSS J0012-1022 after subtractions of the base line components, leading to apparent periodicity around 820 days with significance levels higher than 5σ as shown in middle panel of Fig. 3. Then, the bootstrap method within 2000 loops is applied to determine the periodicity distributions. For each loop, about half of the data points are randomly selected from the original gr-band light curves, leading to the LS re-determined periodicities through the re-created light curves. Distributions of the 2000 re-determined periodicities shown in top left corner of middle panel of Fig. 3 lead to the determined optical periodicity 825±6 days and 826±6 days through the gr-band light curves.

Furthermore, as discussed in Vaughan et al. (2016) and in our recent works in Zhang (2023a,b); Liao et al. (2025); Zhang (2025b), there are apparent effects of red noise (caused by stochastic AGN variability) on detecting optical QPOs. Here, a simple procedure is applied to check the effects of red noise on optical QPOs in SDSS J0012-1022. Accepted the Continuous AutoRegressive (CAR) process described in Kelly et al. (2009) to describe red noise, probability of detecting fake QPOs can be estimated through a series of simulated light curves. The CAR process parameters are the intrinsic variability timescale τ and amplitude σ_*. As well discussed in Kozlowski et al. (2010) for normal quasars, the τ/days can be randomly selected from 100 to 1500, and $\sigma_*/(\mathrm{mag/days}^{0.5})$ can be randomly selected from 0.003 to 0.03. Then, 100000 artificial light curves with the same time information of the ZTF g-band light curve of SDSS J0012-1022 can be created by the CAR process with mean magnitude about 17.5 mags (the mean value of ZTF g-band light curve of SDSS J0012-1022). Then, the LS periodogram is applied to detect optical QPOs with significance level higher than 5σ, and with periodicity within the range from 800 to 850 days, leading to 140 artificial light curves to be selected. Therefore, the probability is only about 0.14% (140/1d5) to detect fake optical QPOs through the CAR process simulated artificial light curves. In other words, the confidence level should be at least higher than 3.2σ to support the detected optical QPOs in SDSS J0012-1022 not from red noise.

Therefore, the optical QPOs with periodicity 827±6 days can be accepted in SDSS J0012-1022, leading the time duration 4487 days from MJD=52141 to 56628 to be $5.43^{+0.03}_{-0.05}$ times of the periodicity. Therefore, for an assumed sub-pc BBH with different phases, there are different spatial structures for the two

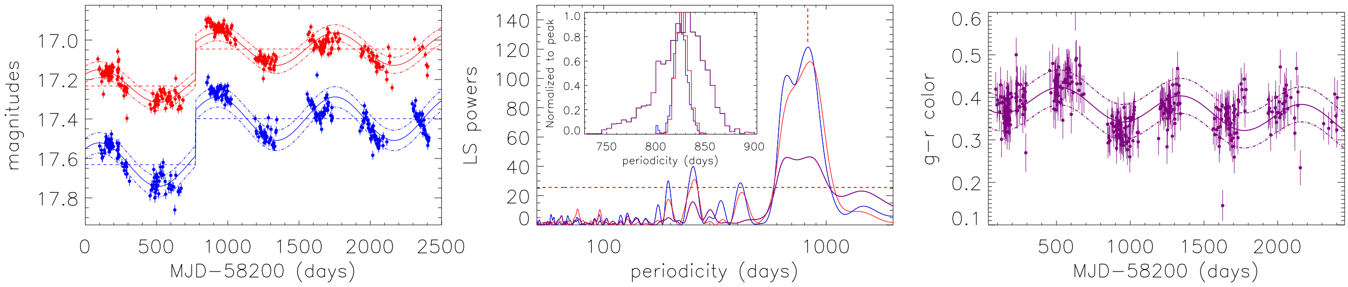

Fig. 3. Left panel shows the ZTF gr-band (in blue and in red) light curves of SDSS J0012-1022. Solid and dot-dashed lines in blue and in red represent the best fitting results and the corresponding 1RMS scatters for the gr-band light curves, horizontal dashed lines in blue and in red show the determined base line components in the gr-band light curves. Middle panel shows the determined LS powers of the gr-band (in blue and in red) light curves and the g-r color (in purple), with horizontal dashed red line representing the 5σ significance level (false alarm probability 3e-7) and with vertical dashed red line marking periodicity=827 days. Top left corner in middle panel shows the bootstrap method determined distributions (in blue, in red and in purple) of the 2000 re-determined periodicities through the ZTF gr-band light curves, and through the g-r color. Right panel shows the g-r color, with solid and dot-dashed lines in purple as the best fitting results and the corresponding 1RMS scatters.

BH accreting systems at the two epochs in SDSS J0012-1022, supporting the discussions on an assumed sub-pc BBH to explain the unique variability of spectral indices in SDSS J0012-1022.

Furthermore, properties of g-r color shown in right panel of Fig. 3 are simply discussed, because the g-r color can be simply applied to trace optical spectral index. The corresponding LS powers of the g-r color shown in the middle panel of Fig. 3 can lead to the determined periodicity 828±23 days, with uncertainty determined by the bootstrap method. Meanwhile, as shown in right panel of Fig. 3, the g-r color can be well modeled by a sine function with periodicity 819±19 days plus a linear trend, leading to the best fitting results with $\chi^2/dof \sim 1.07$. Meanwhile, through the F-test technique applied to compare a sine plus linear model with a linear model, the sine component is preferred with confidence level higher than 10σ as described in Appendix D. The periodicity determined in the g-r color is consistent with the ones determined in the gr-band light curves. Therefore, the QPOs in the g-r color can be accepted as further clues to support our conclusions above, and to further support a central sub-pc BBH in SDSS J0012-1022.

4. Conclusions

Considering time dependent periodic obscurations of central BH accreting systems in sub-pc BBHs, unique variability properties of optical continuum emissions are considered as clues to support central sub-pc BBHs in BLAGN. Through the oversimplified simulations, variability in α_{5100} in multi-epoch spectra leading BLAGN to be outliers in the space of α_{5100} versus L_{5100} could be accepted as clues to support central sub-pc BBHs, such as the results in SDSS J0012-1022 which has unique variability pattern for dependence of α_{5100} on L_{5100} very different from that for normal SDSS quasars. Meanwhile, periodic variations of optical spectral index could be expected in BLAGN harboring assumed sub-pc BBHs. The results in this manuscript open a new window to detect sub-pc BBHs by applications of spectroscopic properties of optical continuum emissions, as well as commonly applied optical QPOs.

Acknowledgements. Zhang gratefully acknowledge the anonymous referee for giving us constructive comments and suggestions to greatly improve the paper. Zhang gratefully thanks the kind financial support from GuangXi University and the kind grant support from NSFC-12173020 and NSFC-12373014 and the support from Guangxi Talent Programme (Highland of Innovation Talents). This manuscript has made use of the data from SDSS (`https://www.sdss.org/`) and ZTF (`https://www.ztf.caltech.edu/`).

References

Almeida, A.; Anderson, S. F.; Argudo-Fernandez, M.; et al., 2023, ApJS, 267, 44
Avara, M. J.; Krolik, J. H.; Campanelli, M.; Noble, S. C.; Bowen, D.; Ryu, T., 2024, ApJ, 974, 242
Arzoumanian, Z., Brazier, A., Burke-Spolaor, S., et al., 2015, ApJ, 813, 65
Begelman, M. C., Blandford, R. D., Rees, M. J., 1980, Natur, 287, 307
Bellm, E. C.; Kulkarni, S. R.; Graham, M. J.; et al., 2019, PASP, 131, 018002
Boroson, T. A., Lauer, T. R. 2009, Nature, 458, 53
Bowen, D. B.; Campanelli, M.; Krolik, J. H.; Mewes, V.; Noble, S. C., 2017, ApJ, 838, 42
Cappellari, M.; Scott, N.; Alatalo, K.; et al., 2013, MNRAS, 432, 1709
Charisi, M.; Bartos, I.; Haiman, Z.; et al., 2016, MNRAS, 463, 2145
D'Orazio, D. J.; Haiman, Z.; Duffell, P.; Farris, B. D.; MacFadyen, A. I., 2015, MNRAS, 452, 2540
Eracleous, M.; Boroson, T. A.; Halpern, J. P.; Liu, J., 2012, ApJS, 201, 23
Fitzpatrick, E. L., 1999, PASP, 111, 63
Foster, R. S., Backer, D. C. 1990, ApJ, 361, 300
Fragione, G.; Grishin, E.; Leigh, N. W. C.; Perets, H. B.; Perna, R., 2019, MNRAS, 488, 47
Graham, M. J.; Djorgovski, S. G.; Stern, D., et al., 2015a, Natur, 518, 74
Graham, M. J., Djorgovski, S. G., Stern, D., et al., 2015b, MNRAS, 453, 1562
Greene, J. E.; Ho, L. C., 2005, ApJ, 627, 721
Izquierdo-Villalba, D.; Sesana, A.; Bonoli, S.; Colpi, M., 2022, MNRAS, 509, 3488
Kelly, B. C.; Bechtold, J.; Siemiginowska, A., 2009, ApJ, 698, 895
Kozlowski, S.; Kochanek, C. S.; Udalski, A.; et al. 2010, ApJ, 708, 927
Liao, G. L.; Chen, X. Q.; Zheng, Q.; Liu Y. L.; Zhang, X. G., 2025, A&A, 698, 265
Masci, F. J.; Laher, R. R.; Rusholme, B.; et al., 2019, PASP, 131, 018003
Mannerkoski, M.; Johansson, P. H.; Rantala, A.; Naab, T.; Liao, S.; Rawlings, A., 2022, ApJ, 929, 167
Markwardt, C. B., 2009, ASPC, 411, 251
Mayer, L.; Kazantzidis, S.; Escala, A.; Callegari, S., 2010, Natur, 466, 1082
Noble, S. C.; Mundim, B. C.; Nakano, H.; Krolik, J. H.; Campanelli, M.; Zlochower, Y.; Yunes, N., 2012, ApJ, 755, 51
Noble, S. C.; Krolik, J. H.; Campanelli, M.; Nakano, H.; Zlochower, Y.; Zilhao, M., 2021, ApJ, 922, 175
Paltani, S.; Courvoisier, T. J. L., 1994, A&A, 291, 74
Patel, P.; Lira, P.; Arevalo, P.; M. Sun, M.; Bernal, S.; Martinez-Aldama, M. L., 2025, A&A, 695, 162
Petrov, P.; Taylor, S. R.; Charisi, M.; Ma, C.-P., 2024, ApJ, 976, 129
Popovic, L. C.; Simic, S.; Kovacevic, A.; Ilic, D.,2021, MNRAS, 505, 5192
Reardon, D. J.; Zic, A.; Shannon, R. M.; et al., 2023, ApJL, 951, L6
Schmidt, K. B.; Rix, H. W.; Shields, J. C.; Knecht, M.; Hogg, D. W.; Maoz, D.; Bovy, J., 2012, ApJ, 744, 147
Sesana, A.; Haiman, Z.; Kocsis, B.; Kelley, L. Z., 2018, ApJ, 856, 42
Shen, Y.; Richards, G. T.; Strauss, M. A.; et al., 2011, ApJS, 194, 45
Somalwar, J. J.; Ravi, V., 2025, ApJ, 982, 195
Truant, R. J.; Izquierdo-Villalba, D.; Sesana, A.; Shaifullah, G. M.; Bonetti, M., 2025, A&A, 694, 282
VanderPlas, J. T., 2018, ApJS, 236, 16
Vaughan, S.; Uttley, P.; Markowitz, A. G.; et al. 2016, MNRAS, 461, 3145
Zechmeister, M.; Kurster, M., 2009, A&A, 496, 577
Zhang, X. G., 2021, MNRAS, 507, 5205, arXiv:2108.09714
Zhang, X. G., 2022a, MNRAS, 512, 1003, arXiv:2202.11995
Zhang, X. G., 2022b, MNRAS, 516, 3650, arXiv:2209.01923
Zhang, X. G., 2023a, MNRAS, 526, 1588, arXiv:2309.08078
Zhang, X. G., 2023b, MNRAS, 525, 335, arXiv:2307.09041
Zhang, X. G., 2025a, ApJ, 983, 90, arXiv:2503.10050
Zhang, X. G., 2025b, ApJ, 979, 147, arXiv:2412.15506
Zhang, X. G., 2025c, A&A Letters accepted, arXiv:2510.14182
Zheng, Z.; Butler, N. R.; Shen, Y.; et al., 2016, ApJ, 827, 56

Appendix A: Two components related to an assumed sub-pc BBH for continuum emissions with MJD=56628

Besides the results shown in top panel of Fig. 1, an extremely oversimplified model has been applied to explain the variability of optical continuum emissions of SDSS J0012-1022. Accepted a central sub-pc BBH in SDSS J0012-1022, for the continuum emissions with MJD=52141, contribution related to one central BH accreting system (the first system) can be obtained without effects of obscurations, but no contribution related to the other one central BH accreting system (the second system) can be obtained due to the second BH accreting system totally obscured by the first system. Then, for the continuum emissions with MJD=56628 in SDSS J0012-1022, due to orbital rotations, continuum emissions from both the central two BH accreting systems can be obtained, but with apparent obscurations on the continuum emissions from the first system which is partly obscured by the second system, and no obscurations on the continuum emissions from the second system which is now the foreground system. Then, even considering the extremely simple conditions, a lot of solutions can be applied to explain the continuum emissions with MJD=56628 in SDSS J0012-1022. Here, accepted E(B-V)~0.1 for the obscurations on the first system, the continuum emissions from the second system can be determined as

$$f_\lambda = (32.51 \pm 0.07) \times (\frac{\lambda}{5100})^{0.32\pm0.02}, \tag{A.1}$$

as shown dashed dark green line in Fig. 2. Meanwhile, based on the corresponding continuum luminosity $\log(L_{5100}/\mathrm{erg/s}) = 44.4$ and spectral index 0.32, the estimated continuum emissions from the second system are similar as the ones in normal quasar SDSS J105635+414602 (plate-mjd-fiberid=1362-53050-0107, $\log(L_{5100}/\mathrm{erg/s}) = 44.46$ and $\alpha_{5100} = 0.32$) listed in the database of Shen et al. (2011). In one word, assumed a central sub-pc BBH in SDSS J0012-1022, unique variability properties of optical spectral index can be explained in SDSS J0012-1022.

Appendix B: Modifications to continuum emissions related to BBHs

As recently discussed in Popovic et al. (2021), relative to effective temperature $T_{(eff,O)}$ from standard accretion disks for normal BLAGN, after considering effects of perturbation of the accretion disc of one BH accreting system due to the gravitational interaction caused by the companion and considering effects of spiral streams accumulating additional materials in each BH accreting system, modified effective temperatures $T_{(eff,i)}$ for the central two BH accreting systems in BBHs can be given as

$$T_{(eff,i)} \sim T_{(eff,O,i)}(1 + q\frac{R_i}{r})^{1/4}(f_{E,i})^{1/4} \quad (i = 1,2) \tag{B.1}$$

with q as BH mass ratio, and r as the distance between the two BH accreting systems, and R as the radius of the part of the perturbed disk component to the central BH of the ith BH accreting system, and $f_{E,i}$ as the ratio of accretion rate to Eddington accretion rate. Therefore, relative to $T_{(eff,O)}$, the modified $T_{(eff,i)}$ are commonly larger, leading to stronger continuum emissions but with common spectral indices. Therefore, considering modified effective temperatures $T_{(eff,i)}$ can lead to the simulated dependence L_A on α_A moving to the upper right with longer distances in top panel of Fig. 1, to further support our conclusions.

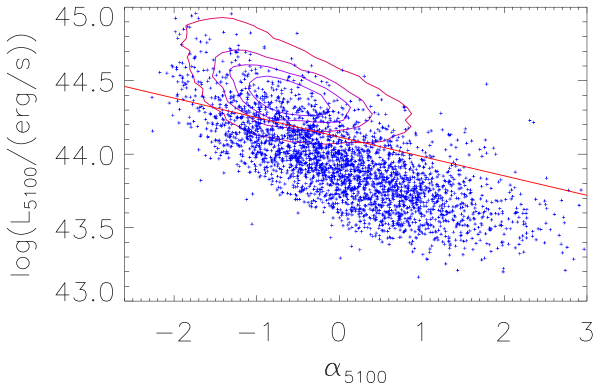

Fig. C.1. Contour with reddish levels represents the same results shown in top panel of Fig. 1 after considering periodic obscurations in assumed sub-pc BBHs. Pluses in blue represent the results from the 3000 newly created artificial f_λ after considering $E_1(B-V,\phi) = E_2(B-V,\phi) = E_0$ with E_0 as a random value between 0 and 0.5. The solid red line shows the dependence determined from SDSS quasars as shown in top panel of Fig. 1.

Appendix C: Effects of periodic obscurations on dependence of L_{5100} versus α_{5100}

Besides the simulated results shown in top panel of Fig. 1, it is necessary to check whether the periodic obscurations have key roles to determine the unique variability of optical spectral index in BLAGN if harbouring central sub-pc BBHS. Here, accepted that the same procedure applied but with a constant extinction by considering $E_1(B-V,\phi) = E_2(B-V,\phi) = E_0$ with E_0 as a random value between 0 and 0.5, the corresponding results are shown in Fig. C.1 based on newly created 3000 artificial f_λ. It can be found that the new results cannot totally cover the same regions of the results with considerations of periodic obscurations, but have more extended areas to the bottom right corner in the space of L_{5100} versus α_{5100}. Therefore, periodic obscurations related to orbital motions have key roles for unique variability properties of optical spectral index in BLAGN if harbouring sub-pc BBHs.

Appendix D: F-test results on the sine component in the g-r color

Besides the best fitting results with $\chi_1^2 = 345.663$ and $dof_1 = 322$ by a sine component plus a linear trend shown in right panel of Fig. 3, only a linear trend has also been applied, leading to $\chi_2^2 = 492.948$ and $dof_2 = 325$. Therefore, through the F-test technique, the calculated value F_p is about

$$F_p = \frac{\frac{\chi_2^2 - \chi_2^1}{dof_2 - dof_1}}{\chi_1^2/dof_1} = 45.73 \tag{D.1}$$

. Meanwhile, considering $dof_2 - dof_1 = 3$ and $dof_1 = 322$ as the number of dofs of the F distribution numerator and denominator, the F distribution expected value with 10σ confidence level is about 20 which is smaller than $F_p = 45.73$. Therefore, the sine component included in the g-r color is preferred with confidence level higher than 10σ.